European Journal of Medicinal Chemistry 71 (2014) 148–159

Contents lists available at ScienceDirect

European Journal of Medicinal Chemistry

journal homepage: http://www.elsevier.com/locate/ejmech

Original article

Synthesis and biological evaluation of α-triazolyl chalcones as a new type of potential antimicrobial agents and their interaction with calf thymus DNA and human serum albumin

Ben-Tao Yin, Cong-Yan Yan, Xin-Mei Peng, Shao-Lin Zhang, Syed Rasheed [1], Rong-Xia Geng*, Cheng-He Zhou*

Laboratory of Bioorganic & Medicinal Chemistry, School of Chemistry and Chemical Engineering, Southwest University, Chongqing 400715, People's Republic of China

ARTICLE INFO

Article history:
Received 7 June 2013
Received in revised form
29 October 2013
Accepted 2 November 2013
Available online 9 November 2013

Keywords:
Chalcone
Triazole
Antibacterial
Antifungal
Calf thymus DNA
Human serum albumin

ABSTRACT

A series of α-triazolyl chalcones were efficiently synthesized. Most of the prepared compounds showed effective antibacterial and antifungal activities. Noticeably, α-triazolyl derivative **9a** exhibited low MIC value of 4 μg/mL against MRSA and *Micrococcus luteus*, which was comparable or even superior to reference drugs. The further research revealed that compound **9a** could effectively intercalate into Calf Thymus DNA to form **9a**–DNA complex which might block DNA replication to exert their powerful antimicrobial activities. Competitive interactions between **9a** and metal ions to Human Serum Albumin (HSA) suggested the participation of Fe^{3+}, K^{+} and Mg^{2+} ions in **9a**–HSA system could increase the concentration of free **9a**, shorten its storage time and half-life in the blood, thus improving its antimicrobial efficacy.

1. Introduction

The incidence of invasive life-threatening infections has been increasing dramatically in recent two decades [1,2]. Particularly, the emergence of multi-drug resistant strains such as methicillin-resistant *Staphylococcus aureus* (MRSA) has been a serious problem of ever-increasing significance in both community and hospital acquired infections [3]. Therefore, there is a really perceived need to develop novel compounds with completely distinct skeleton structure from those of well-known classes of antimicrobial agents to which many clinically relevant pathogens are now resistant. Consequently, the search for new molecular scaffolds with high efficiency, broad spectrum and low toxicity will always remain an important and challenging task for medicinal chemists.

Chalcones with a structural characteristic of the typical diaryl enone scaffold are an important class of natural and synthetic bioactive compounds possessing a variety of biological activities [4–9]. Especially in antibacterial [10] and antifungal [11] aspects, chalcones have shown large potentiality in the treatment of infective diseases. An increasing number of efforts have been devoted to their isolation, artificial synthesis and biological evaluation. Licochalcone A (**1**), a natural chalcone product, showed potent antibacterial activity especially against *Bacillus subtilis*, *S. aureus* and *Micrococcus luteus* [12]. In recent years, the introduction of heterocycles into chalcone as antimicrobial agents has attracted extensive interest. Chalcone **2** containing oxazolidone exhibited surprisingly much higher efficiencies towards MRSA and vancomycin-resistant *Enterococcus faecalis* (VRE) than Linezolide [13]. Thiazolidinedione substituted chalcone **3** also gave 8-fold (MIC = 1 μg/mL) and 64-fold (MIC = 0.5 μg/mL) more potential activities against MRSA CCARM3167 and 3506 respectively in contrast to Norfloxacin (MIC = 8 and 4 μg/mL) and Oxacillin (MIC > 64 μg/mL) [14]. Imidazole modified chalcones **4a** and **4b** showed comparable activity against *Aspergillus fumigatus* to the reference antibiotic nystatin [15]. Tetrazole linked chalcones **5a**–**b** gave better anti-*S. aureus* and anti-*Escherichia coli* activities than Ciprofloxacin and considerably high

* Corresponding authors. Tel./fax: +86 23 68254967.
E-mail addresses: geng0712@swu.edu.cn (R.-X. Geng), zhouch@swu.edu.cn, zhouch6848@sina.com (C.-H. Zhou).
[1] Postdoctoral fellow from Department of Chemistry, University of Hyderabad, India.

0223-5234/$ – see front matter © 2013 Elsevier Masson SAS. All rights reserved.
http://dx.doi.org/10.1016/j.ejmech.2013.11.003

potencies against *C. albicans* and *A. niger* in comparison with Griseofulvin [16]. The above observations showed that the introduction of heterocycles into chalcone skeleton is of great development value as potential antimicrobial agents, which has provoked considerable interest to develop chalcone-based compounds as new antimicrobial drugs (Fig. 1) [17].

Triazole nucleus with three nitrogen atoms and electron rich property has been paid special attention in the development of new drugs due to large medicinal potentiality of triazole-based derivatives [18–21]. A lot of triazole Antifungal drugs such as Fluconazole, Terconazole and Itraconazole have been extensively used in clinic [22–24]. These exciting achievements encourage continuous efforts to develop novel triazole compounds for the treatment of infective diseases. Considering the importance of chalcone and triazole compounds, and as an extension of our researches on bioactive heterocyclic compounds [25–33], herein, a series of α-triazolyl chalcone derivatives as a structurally new type of potential antimicrobial agents were designed and synthesized. The target compounds were designed on the basis of the following considerations:

(1) The combination of nitrogen heterocyclic rings with chalcones, and the replacement or modification of the aromatic ring in chalcones as antimicrobial agents have been reported actively and shown large development potentiality. However, the modification of diaryl enone scaffold especially at α-position has been rarely reported. Therefore, a series of α-triazole chalcones were designed and synthesized as novel structural type of potential antimicrobial agents.
(2) Triazole moiety is able to easily bind with various enzymes and receptors in organisms through coordination bonds, hydrogen bonds, ion-dipole, cation-π, π–π stacking, hydrophobic effect and van der Waals force *etc.*, which helpfully modulate the physicochemical and pharmacokinetics properties. Rationally, triazole moiety was introduced into the skeleton of chalcone, the resulting derivatives might be able to play a positive role in treating microbial infections.
(3) Much research has revealed that substituents in aromatic ring could significantly influence the bioactivities by regulating the lipid-water partition coefficient and binding affinity. So various substituted α-triazole chalcones were prepared with the aim to explore the effect of substituents on biological activity.

All the newly synthesized compounds were characterized by modern spectra and evaluated for their antibacterial and antifungal activities *in vitro* against four Gram-positive bacteria, four Gram-negative bacteria and two fungi.

It has been reported that the interactions between drugs or bioactive small molecules and deoxyribonucleic acid (DNA) or human serum albumin (HSA) are beneficial not only to provide a proper understanding of the absorption, transportation, distribution, metabolism, excretion properties and possible mechanism of agents, but also to design, modify and screen drug molecules. DNA is viewed as the informational molecule used in the development and function of almost all the known living organisms. There is growing interest in exploring the binding of small molecules with DNA for the rational design and construction of new and efficient drugs. The affinity between drugs and HSA can change the overall distribution, metabolism, and efficacy of drugs, and many promising new drugs have been rendered ineffective because they have too high or low affinity to this protein. So the preliminary antimicrobial mechanism, transportation and pharmacokinetic properties were investigated by evaluating the interaction of the prepared highly active compound with calf thymus DNA and HSA [34–39].

2. Results and discussion

2.1. Chemistry

The synthetic route of α-triazolyl chalcones was outlined in Scheme 1. The desired target compounds were synthesized *via* multistep reactions from commercially available substituted benzenes, chloroacetyl chloride, 1,2,4-triazole and aromatic aldehydes. Intermediates **6a–d**, prepared by Friedel–Crafts acylation of substituted benzenes **5a–d** with chloroacetyl chloride in dichloromethane, and then reacted with 1,2,4-triazole by *N*-alkylation to produce compounds **7a–d** in good yields of 69.1–95.3% [24]. The reaction of intermediates **7a–d** respectively with aromatic aldehydes *via* aldol condensation in toluene catalyzed by glacial acetic acid and piperidine afforded the target compounds **8a–j**.

α-Triazolyl chalcone **8e** was obtained in 71.0% yield by the condensation of compound **7d** with equimolar benzaldehyde in toluene in the presence of catalytic amount of both piperidine and glacial acetic acid. However, to our surprise, another new compound was obtained in 16.0% yield. Spectral and X-ray diffraction analyses showed to be the piperidyl substituted α-triazolyl chalcone **9a** (Fig. 2). The fluorine atom at 2′-position of benzene ring in chalcone **8e** was surprisingly substituted by piperidyl group in spite of larger hindrance than the corresponding 4′-position, and the *Z* configuration and *s-trans* conformation were adopted due to the presence of triazole ring that probably decreased the rotational flexibility of the

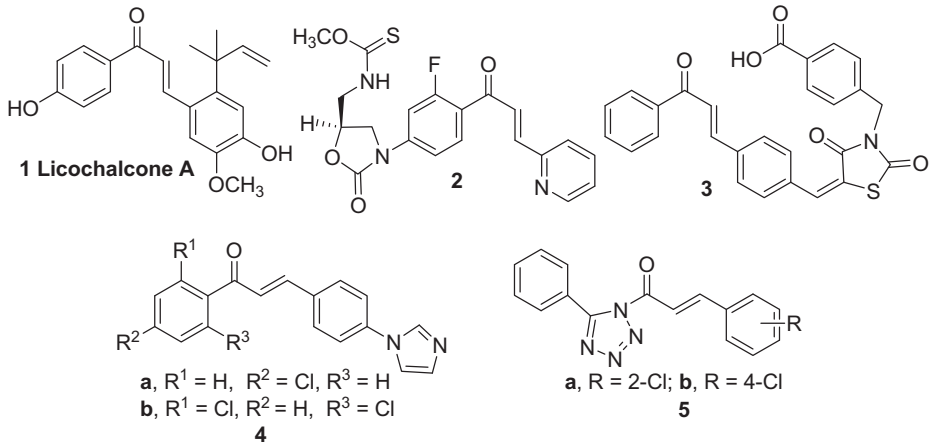

Fig. 1. Structures of some antimicrobial chalcone derivatives.

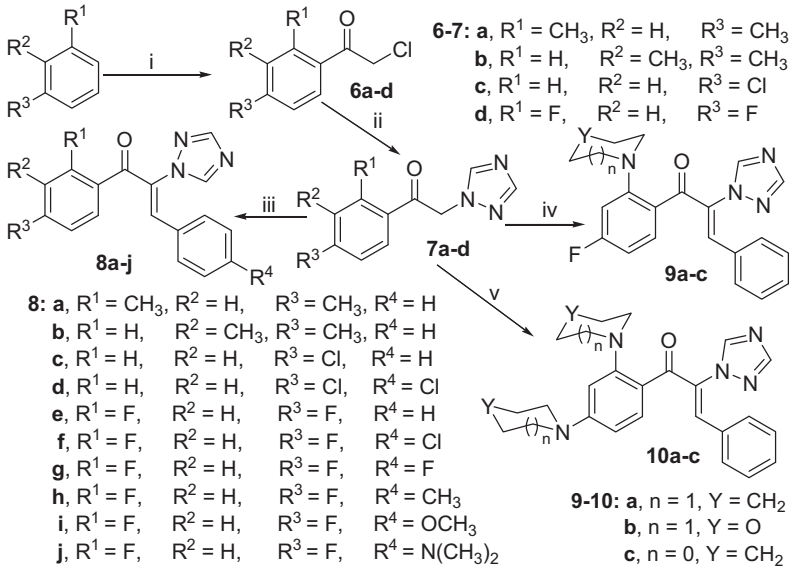

Reagents and conditions: (i) $ClCOCH_2Cl$, $AlCl_3$, CH_2Cl_2, rt, 2–3 h; (ii) 1,2,4-Triazole, K_2CO_3, CH_3CN, rt–80 ℃, 1-2 h; (iii) Aryl aldehyde, glacial acetic acid and piperidine, toluene, refluxed, 6–8 h, yields 45.9–89.4%; (iv-v) Triazolyl acetophenone : Benzaldehyde : Cyclic amines = 1 : 1 : 2, toluene, refluxed, 8–10 h, yields 13.1–53.4%.

Scheme 1. Synthetic route of target compounds.

single bond in enone linkage. As a comparison, the single crystal of chalcone **8e** was also gained and its structure was showed in Fig. 2.

In order to enhance the yield of 2′-piperidyl α-triazolyl chalcone **9a**, the molar ratio of piperidine and compound **7d** was augmented to 2, chalcone **9a** was obtained as predominance accompanying with another yellow piperidyl bis-substituted chalcone **10a** (Sheme 1). Some other cyclic aliphatic amines such as pyrrolidine and morpholine also successfully accessed mono-substituted cyclic aliphatic amino α-triazolyl chalcones **9b**–**c** and bis-substituted ones **10b**–**c**. All the newly synthesized compounds were characterized by ^1H NMR, ^{13}C NMR, IR, MS and HRMS spectra and some of them were further confirmed by X-ray diffraction and HSQC spectra (Supplementary information).

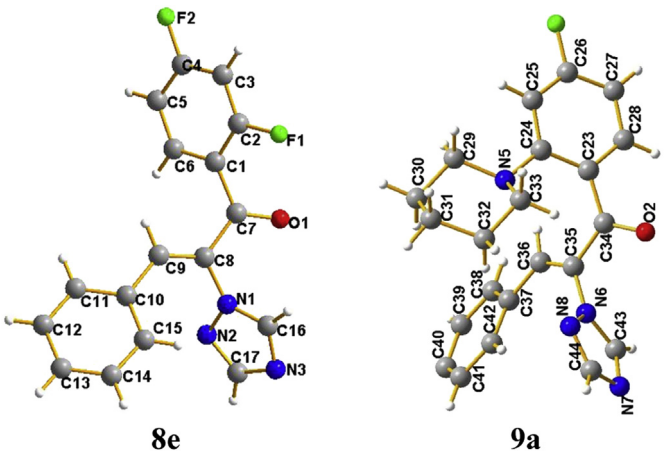

Fig. 2. X-ray structures of α-triazolyl chalcones **8e** and **9a**.

2.2. Biological activity

The *in vitro* antimicrobial activities of all the target chalcones **8**–**10** were evaluated against four Gram-positive bacteria (MRSA, *S. aureus* ATCC 25923, *B. subtilis* ATCC 21216, and *M. luteus* ATCC 4698), four Gram-negative bacteria (*E. coli* JM109, *Bacillus typhi*, *P. aeruginosa* ATCC 27853 and *Bacillus proteus* ATCC 13315) and two fungi (*C. albicans* ATCC 76615 and *C. mycoderma* ATCC 96918) using two-fold broth dilution method (Supplementary information) in 96-well micro-test plates recommended by National Committee for Clinical Laboratory Standards (NCCLS) [40]. Clinical antimicrobial drugs Chloromycin, Norfloxacin and Fluconazole are used as the positive control.

2.2.1. Antibacterial activity

The antibacterial assay showed that compounds **8a**–**j**, **9a**–**c** and **10a**–**c** exhibited moderate to excellent efficacy against all the tested bacterial strains. Noticeably, compound **9a** displayed remarkable antibacterial activities in comparison to Chloromycin and Norfloxacin, which indicated that compound **9a** should have large possibility as potent novel antimicrobial agent.

Table 1 showed valuable effects of halo substituents on biological activities. Most of halo-substituted α-triazolyl chalcones were more active against the tested bacteria than non-halo substituted ones. Particularly, compound **8d** with 4-chlorobenzyl group gave stronger inhibition against *E. coli* (MIC = 16 μg/mL) and *Bacillus typhi* (MIC = 16 μg/mL) than Chloromycin (MIC = 32 μg/mL), and also it possessed superior anti-*P. aeruginosa* (MIC = 8 μg/mL) efficiency to Norfloxacin (MIC = 16 μg/mL). When electron-donating groups were introduced, surprisingly, only methoxy modified chalcone **8i** was observed slightly enhanced activities. It exhibited better anti-MRSA efficiency (MIC = 4 μg/mL) than Chloromycin (MIC = 16 μg/mL) and Norfloxacin (MIC = 8 μg/mL).

Among the cyclic amino substituted α-triazolyl chalcones **9a**–**c** and **10a**–**c**, mono-substituted derivatives **9a**–**c** were more active than bis-substituted compounds **10a**–**c**. This might be resulted

Table 1
Antimicrobial data as MIC (μg/mL)[a,b] for α-triazolyl chalcones **8**–**10**.

Compds	Gram-positive bacteria				Gram-negative bacteria				Fungi	
	MRSA	*S. aureus*	*B. subtilis*	*M. luteus*	*E. coli*	*B. typhi*	*P. aeruginosa*	*B. proteus*	*C. albicans*	*C. mycoderma*
8a	64	128	128	256	256	128	256	128	128	256
8b	256	256	64	128	16	128	128	128	16	256
8c	32	64	64	64	128	64	256	64	16	64
8d	32	32	32	64	16	16	8	32	64	64
8e	64	32	64	64	32	32	128	64	128	64
8f	32	16	32	64	64	32	128	64	16	16
8g	128	64	64	32	32	32	32	16	64	64
8h	32	32	64	64	32	64	16	64	16	16
8i	4	8	8	16	16	32	16	8	16	32
8j	32	64	64	64	128	64	256	64	16	64
9a	4	16	8	4	16	8	16	8	16	8
9b	128	32	32	64	16	32	64	32	128	32
9c	16	16	8	16	8	4	16	16	32	256
10a	32	16	32	64	64	32	128	64	16	16
10b	64	32	64	64	32	32	128	64	128	64
10c	16	32	16	16	32	8	32	32	8	4
Chloromycin	16	16	32	8	32	32	32	32	–	–
Norfloxacin	8	0.5	1	2	16	4	16	8	–	–
Fluconazole	–	–	–	–	–	–	–	–	1	4

[a] Minimum inhibitory concentrations were determined by micro broth dilution method for microdilution plates.
[b] MRSA, Methicillin-Resistant *Staphylococcus aureus* (N315); *S. aureus*, *Staphylococcus aureus* (ATCC25923); *B. subtilis*, *Bacillus subtilis*; *M. luteus*, *Micrococcus luteus* (ATCC4698); *E. coli*, *Escherichia coli* (JM109); *B. typhi*, *Bacillus typhi*; *P. aeruginosa*, *Pseudomonas aeruginosa*; *B. proteus*, *Bacillus proteus* (ATCC13315); *C. albicans*, *Candida albicans* (ATCC76615); *C. mycoderma*, *Candida mycoderma*.

from the better water-solubility of **9a**–**c**. Compounds **9a** and **9c** possessed good efficiencies in inhibiting the growth of *Micrococcus luteus B. subtilis*, *P. aeruginosa* and *Bacillus proteus*, which were equivalent or superior to the reference drug Chloromycin. Notably, compound **9a** also exhibited broad-spectrum and good antibacterial efficacies with MICs between 4 and 16 μg/mL, and its anti-MRSA ability (MIC = 4 μg/mL) was better than Chloromycin (MIC = 16) and Norfloxacin (MIC = 8 μg/mL).

2.2.2. Antifungal activity

The *in vitro* antifungal data (Table 1) indicated that all target chalcones displayed moderate inhibitory potencies against two tested fungi. It was obviously found that the antifungal abilities of the synthesized compounds displayed similarity to their antibacterial efficiency. Moreover, the fungus *C. mycoderma* was more sensitive than *C. albicans*, and bis-pyrrolidyl chalcone **10c** showed the strongest inhibition towards *C. mycoderma*, equivalent to the reference drug Fluconazole with MIC value of 4 μg/mL. Furthermore, bis-piperidyl chalcone **10a** exhibited relatively notable efficacy in inhibiting the growth of tested fungi, suggesting that chalcone with bis-cyclic amino substituent can be served as an attractive stimulus for further investigation.

2.3. Interactions with calf thymus DNA

DNA is one of the targets for the studies of biologically important small molecules such as antimicrobial drugs. There is growing interest in investigating the interaction of small molecules with DNA for the rational design and construction of new and efficient drugs targeted to DNA. To explore the possible antimicrobial action mechanism, the binding behavior of compound **9a** with calf thymus DNA (a DNA model with medical importance, low cost and ready availability properties) was studied on molecular level *in vitro* using neutral red (NR) dye as a spectral probe by UV–vis spectroscopic methods.

2.3.1. Absorption spectra of DNA in the presence of compound *9a*

The application of absorption spectroscopy is one of the most useful techniques in DNA-binding studies. In absorption spectroscopy, hypochromism and hyperchromism are very important spectral features to distinguish the change of DNA double-helical structure. Due to the strong interaction between the electronic states of intercalating chromophore and that of the DNA base, the observed large hypochromism strongly suggests a close proximity of the aromatic chromophore to the DNA bases. With a fixed concentration of DNA, UV–vis absorption spectra were recorded with the increasing amount of compound **9a**. As shown in Fig. 3, UV–vis spectra displayed that the maximum absorption peak of DNA at 260 nm exhibited proportional increase with the increasing concentration of compound **9a**. Meanwhile the absorption value of simply sum of free DNA and free compound **9a** was a little greater than the measured value of **9a**–DNA complex. These meant a weak hypochromic effect existed between DNA and compound **9a**. Furthermore, the intercalation of the aromatic chromophore of compound **9a** into the helix and the strong overlap of π–π* states

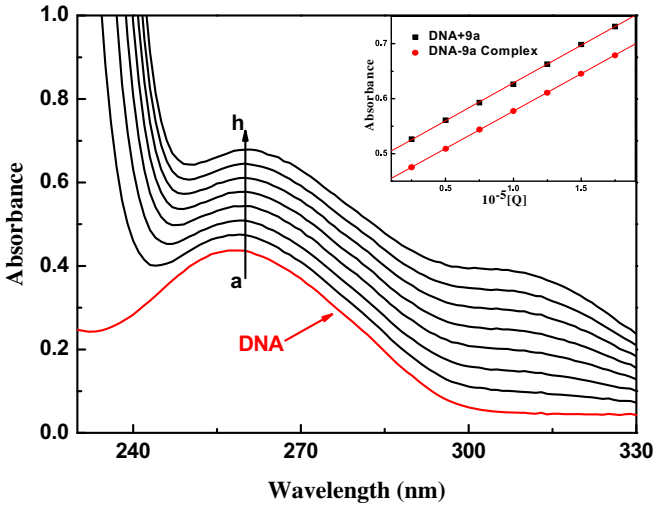

Fig. 3. UV absorption spectra of DNA with different concentrations of compound **9a** (pH = 7.4, T = 290 K). Inset: comparison of absorption at 260 nm between the **9a**–DNA complex and the sum values of free DNA and free compound **9a**. c(DNA) = 5.95 × 10^{-5} mol/L, and c(compound **9a**) = 0–1.75 × 10^{-5} mol/L for curves *a*–*h* respectively at increment 0.25 × 10^{-5}.

in the large π-conjugated system with the electronic states of DNA bases were consistent with the observed spectral changes [38,39].

On the basis of the variations in the absorption spectra of DNA upon binding to **9a**, equation (1) can be utilized to calculate the binding constant (K).

$$\frac{A^0}{A-A^0} = \frac{\xi_C}{\xi_{D-C}-\xi_C} + \frac{\xi_C}{\xi_{D-C}-\xi_C} \times \frac{1}{K[Q]} \quad (1)$$

A^0 and A represent the absorbance of DNA in the absence and presence of compound **9a** at 260 nm, ξ_C and ξ_{D-C} are the absorption coefficients of compound **9a** and **9a**–DNA complex respectively. The plot of $A^0/(A - A^0)$ versus 1/[compound **9a**] is constructed by using the absorption titration data and linear fitting (Fig. 4), yielding the binding constant, $K = 1.22 \times 10^4$ L/mol, $R = 0.999$, SD = 0.12 (R is the correlation coefficient. SD is standard deviation).

2.3.2. Absorption spectra of NR interaction with DNA

Neutral Red (NR) is a planar phenazine dye and is structurally similar to other planar dyes, for example, those of the acridine, thiazine, and xanthene kind. It has been demonstrated that the binding of NR with DNA is an intercalation binding in recent years. Therefore, NR was employed as a spectral probe to investigate the binding mode of **9a** with DNA in the present work.

The absorption spectra of the NR dye upon the addition of DNA are showed in Fig. 5. It is apparent that the absorption peak of the NR at around 460 nm showed gradual decrease with the increasing concentration of DNA, and a new band at around 530 nm developed. This was attributed to the formation of the new DNA–NR complex. An isosbestic point at 504 nm provided evidence of DNA–NR complex formation.

2.3.3. Absorption spectra of competitive interaction of compound *9a* and NR with DNA

Fig. 6 displayed the absorption spectra of a competitive binding between NR and **9a** with DNA. As shown, with the increasing concentration of **9a**, the maximum absorption around 530 nm of the DNA–NR complex decreased, but a slight intensity increase was observed in the developing band around 460 nm. Compared with the absorption band at around 460 nm of the free NR in the presence of the increasing concentrations of DNA (Fig. 5), the spectra in Fig. 6 (inset) exhibited the reverse process. The results suggested

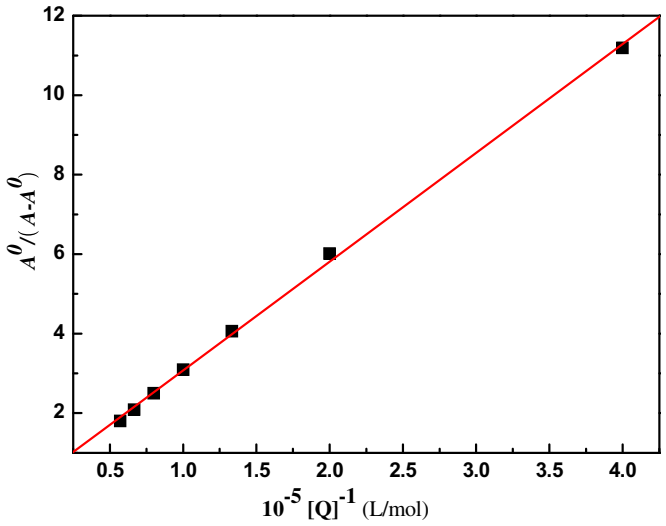

Fig. 4. The plot of $A^0/(A - A^0)$ versus 1/[compound **9a**].

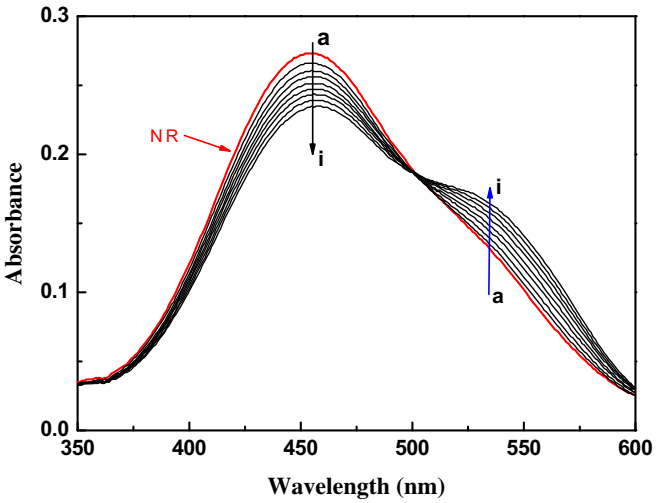

Fig. 5. UV absorption spectra of NR in the presence of DNA at pH 7.4 and room temperature. c(NR) = 2 × 10^{-5} mol/L, and c(DNA) = 0–3.81 × 10^{-5} mol/L for curves a–i respectively at increment 0.48 × 10^{-5}.

that compound **9a** intercalated into the double helix of DNA by substituting for NR in the DNA–NR complex.

2.4. Interactions of compound *9a* with HSA

HSA is the principal extracellular protein of the circulatory system, and accounts for about 60% of the total plasma proteins corresponding to a concentration of 42 mg/mL and provides about 80% of the colloid osmotic pressure of blood. It is well accepted that the overall distribution, metabolism, and efficacy of drugs can be changed by their affinity to HSA, and many promising new drugs have been rendered ineffective because of their unusually high affinity to this protein. So the investigations of interactions between drugs or bioactive small molecules and HSA are not only beneficial to provide a proper understanding of the absorption, transportation, distribution,

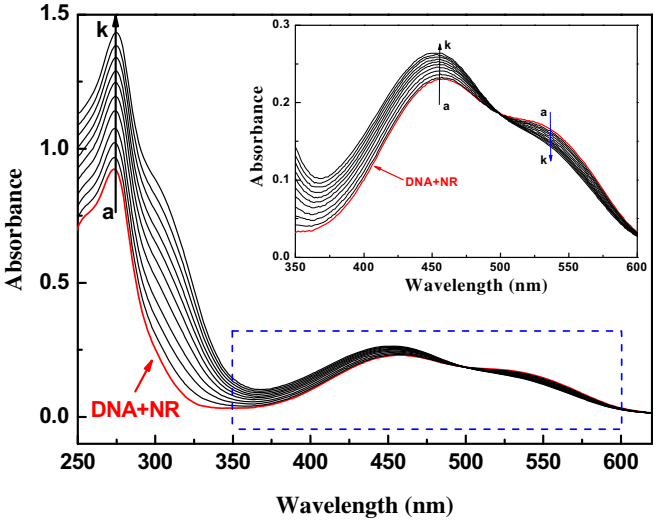

Fig. 6. UV absorption spectra of the competitive reaction between **9a** and neutral red with DNA. c(DNA) = 4.17 × 10^{-5} mol/L, c(NR) = 2 × 10^{-5} mol/L, and c(compound **9a**) = 0–2.5 × 10^{-5} mol/L for curves a–k respectively at increment 0.25 × 10^{-5}. (Inset) Absorption spectra of the system with the increasing concentration of **9a** in the wavelength range of 350–600 nm absorption spectra of competitive reaction between compound **9a** and NR with DNA.

metabolism and excretion properties of drugs, but also significant to design, modify and screen drug molecules.

2.4.1. UV–vis absorption spectral study

UV–vis absorption measurement is a very easy operational method applicable to explore the structural change of protein and to identify the complex formation. In our binding experiment, UV–vis absorption spectroscopic method was adopted to evaluate the binding behaviors between compound **9a** and HSA. As shown in Fig. 7, the absorption peak observed at 278 nm was attributed to the aromatic rings in Tryptophan (Trp-214), Tyrosine (Tyr-411) and Phenylalanine (Phe) residues in HSA. With the addition of compound **9a**, the peak intensity increased, indicating that compound **9a** could interact with HSA and the peptide strands of HSA were extended. However, the maximum absorption wavelength remained unchanged, implying that the interactions of compound **9a** and HSA was a noncovalent interaction, which occurred *via* the π–π stacking between aromatic rings of compound **9a** and Trp, Tyr and Phe residues possessed conjugated π-electrons and located in the binding cavity of HSA [41].

2.4.2. Fluorescence quenching mechanism

Fluorescence spectroscopy is also an effective method to study the interactions of small molecules with HSA. The fluorescence intensity of Trp-214 may change when HSA interacts with other small molecules, which could be reflected in the fluorescence spectra of HSA in the UV region. The effect of compound **9a** on the fluorescence intensity to HSA at 298 K was shown in Fig. 8. It was obvious that HSA had a strong fluorescence emission with a peak at 348 nm owing to the single Try-214 residue. The intensity of this characteristic broad emission band regularly decreased with the increased concentrations of compound **9a**, but the maximum emission wavelength of HSA remained unchanged. This suggested that Trp-214 did not undergo any change in polarity, and hence compound **9a** was likely to interact with HSA *via* the hydrophobic region located in HSA [34].

The fluorescence quenching data can be analyzed by the well-known Stern–Volmer equation [42]:

$$\frac{F_0}{F} = 1 + K_{SV}[Q] = 1 + K_q\tau_0[Q] \quad (2)$$

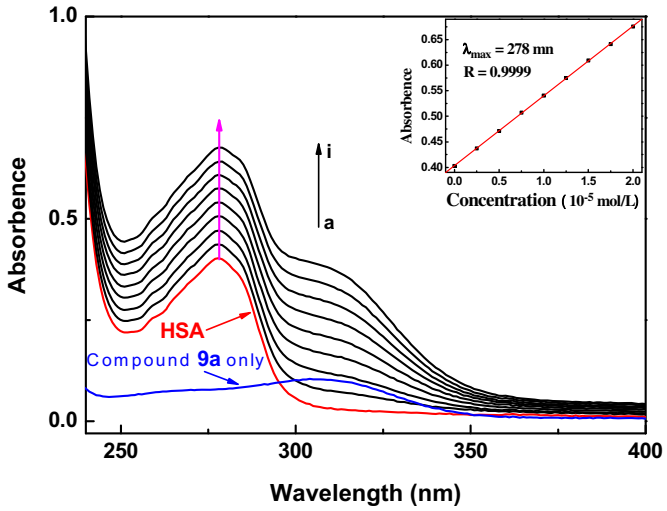

Fig. 7. Effect of compound **9a** to HSA UV–vis absorption, c(HSA) = 1.0 × 10^{-5} mol/L; c(compound **9b**)/(10^{-5} mol/L): 0, 0.25, 0.5, 0.75, 1, 1.25, 1.5, 1.75, 2, (T = 298 K, pH = 7.4). The inset corresponds to the absorbance at 278 nm with different concentrations of compound **9a**.

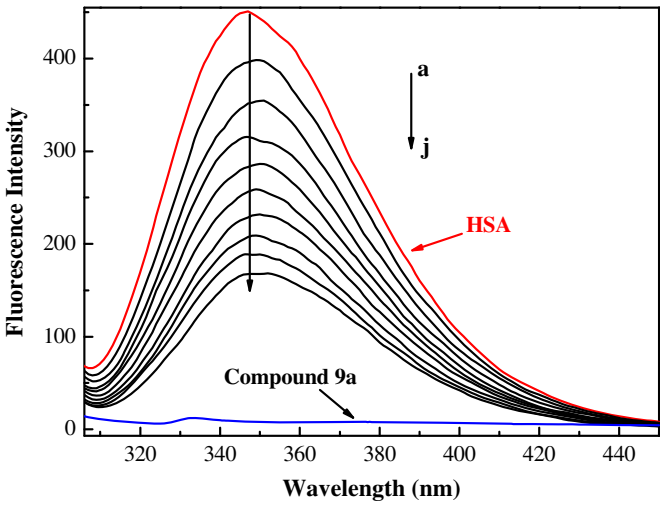

Fig. 8. Emission spectra of HSA in the presence of various concentrations of compound **9a**. c(HSA) = 1.0 × 10^{-5} mol/L; c(compound **9a**)/(10^{-5} mol/L), a–j: from 0.0 to 2.25 at increments of 0.25; blue line shows the emission spectrum of compound **9a** only; T = 298 K, λ_{ex} = 295 nm. (For interpretation of the references to color in this figure legend, the reader is referred to the web version of this article.)

where F_0 and F represent fluorescence intensity in the absence and presence of compound **9a**, respectively. K_{SV} (L/mol) is the Stern–Volmer quenching constant, K_q is the bimolecular quenching rate constant (L mol^{-1} s^{-1}), τ_0 is the fluorescence lifetime of the fluorophore in the absence of quencher, assumed to be 6.4 × 10^{-9} s for HSA, and [Q] is the concentration of compound **9a**. Hence, the Stern–Volmer plots of HSA in the presence of compound **9a** at different concentrations and temperatures could be calculated and were showed in Fig. 9.

Fluorescence quenching occurs by different mechanisms, usually classified as dynamic quenching and static quenching depending on temperature and viscosity. Because higher temperatures result in larger diffusion coefficients, the quenching constants are expected to increase with a gradually increasing temperature in dynamic quenching. However, the increase of temperature is likely to result in a smaller static quenching constant due to the dissociation of weakly bound complexes.

The values of K_{SV} and K_q for the interaction of compound **9a** with HSA at different temperatures were showed in Table 2. The K_{SV}

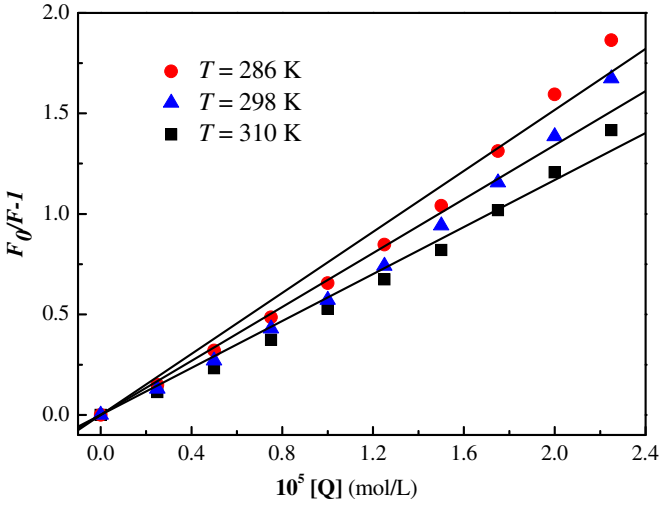

Fig. 9. Stern–Volmer plots of **9a**–HSA system at different temperatures.

Table 2
Stern–Volmer quenching constants for the interaction of compound **9a** with HSA at various temperatures.

pH	T (K)	K_{SV} (L/mol)	K_q (L mol^{-1} s^{-1})	R^a	S.D.^{b}
7.4	286	7.59×10^4	1.19×10^{13}	0.993	0.090
	298	6.72×10^4	1.05×10^{13}	0.993	0.084
	310	5.84×10^4	9.13×10^{12}	0.996	0.058

R^a is the correlation coefficient.
S.D.^{b} is standard deviation.

values were inversely correlated with the temperature, which indicated that the fluorescence quenching of HSA was probably initiated by the formation of **9a**–HSA complex rather than dynamic collisions. The K_q values obtained at different temperatures were in the range of 10^{12}–10^{13} L mol^{-1} s^{-1} (Table 3), which far exceeded the diffusion controlled rate constants of various quenchers with a biopolymer (2.0×10^{10} L mol^{-1} s^{-1}), and indicated that the quenching was not initiated by the dynamic diffusion process but occurred in the statical formation of **9a**–HSA complex [34].

2.4.3. Binding constant and sitesss

For a static quenching process, the data could be described by the Modified Stern–Volmer equation [43]:

$$\frac{F_0}{\Delta F} = \frac{1}{f_a K_a}\frac{1}{[Q]} + \frac{1}{f_a} \quad (3)$$

Where ΔF is the difference in fluorescence intensity in the absence and presence of compound **9a** at concentration [Q], f_a is the fraction of accessible fluorescence, and K_a is the effective quenching constant for the accessible fluorophores, which are analogous to associative binding constants for the quencher-acceptor system. The dependence of $F_0/\Delta F$ on the reciprocal value of quencher concentration $[Q]^{-1}$ is linear with the slope equaling to the value of $(f_a K_a)^{-1}$. The value f_a^{-1} is fixed on the ordinate. The constant K_a is a quotient of the ordinate f_a^{-1} and the slope $(f_a K_a)^{-1}$. The Modified Stern–Volmer plots were showed in Fig. 10 and the calculated results were depicted in Table 3.

When small molecules bind to a set of equivalent sites on a macromolecule, the equilibrium binding constants and the numbers of binding sites can also be calculated according to the Scatchard equation [44]:

$$r/D_f = nK_b - rK_b \quad (4)$$

where D_f is the molar concentration of free small molecules, r is the moles of small molecules bound per mole of protein, n is binding sites multiplicity per class of binding sites, and K_b is the equilibrium binding constant. The Scatchard plots were showed in Fig. 11 and the K_b and n were listed in Table 3.

Fig. 11 showed the Modified Stern–Volmer and Scatchard plots for the **9a**–HSA system at different temperatures. The decreased trend of K_a and K_b with increased temperatures was in accordance with K_{SV}'s depended on temperatures. The value of the binding site n was approximately 1, which showed one high affinity binding site was present in the interaction of compound **9a** with HSA. The

Table 3
Binding constants and sites of **9a**–HSA system at pH = 7.4

T (K)	Modified Stern–Volmer method			Scatchard method			
	$10^{-4}K_a$ (L/mol)	R	S.D	$10^{-4}K_b$ (L/mol)	R	S.D.	n
286	4.54	0.999	0.046	4.60	0.996	0.008	1.27
298	3.64	0.999	0.027	3.64	0.998	0.005	1.38
310	2.95	0.999	0.044	3.03	0.995	0.006	1.45

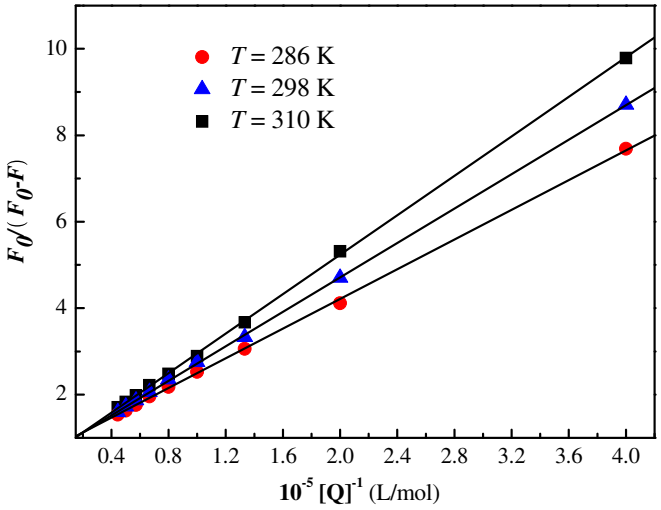

Fig. 10. Modified Stern–Volmer plots of **9a**–HSA system at different temperatures.

results also showed that the binding constants were moderate and the effects of temperatures were not significant, thus compound **9a** might be stored and carried by this protein.

2.4.4. Binding mode and thermodynamic parameters

Generally, there are four types of non-covalent interactions including hydrogen bonds, van der Waals forces, electrostatic interactions and hydrophobic bonds, which play important roles in small molecules binding to proteins [45]. The thermodynamic parameters enthalpy (ΔH) and entropy (ΔS) change of binding reaction are the main evidence for confirming the interactions between small molecules and protein. If the ΔH does not vary significantly over the studied temperatures range, then its value and ΔS can be evaluated from the van't Hoff equation:

$$\ln K = -\frac{\Delta H}{RT} + \frac{\Delta S}{R} \quad (5)$$

where K is analogous to the associative binding constants at the corresponding temperature and R is the gas constant. In order to explain the binding model between compound **9a** and HSA, the thermodynamic parameters were calculated from the van't Hoff plots. The ΔH was estimated from the slope of the van't Hoff

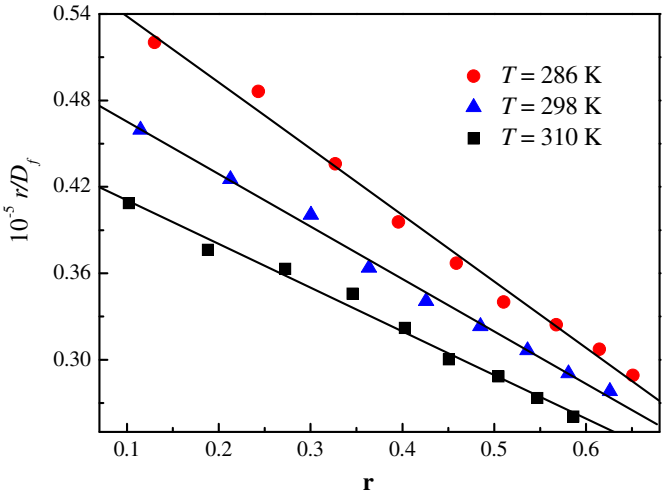

Fig. 11. Scatchard plots of **9a**–HSA system at different temperatures.

relationship (Fig. 12). The free energy change (ΔG) was then calculated from the following equation:

$$\Delta G = \Delta H - T\Delta S \quad (6)$$

Table 4 summarized the values of ΔH, ΔG and ΔS. The negative values of free energy ΔG of the interaction between compound **9a** and HSA suggested that the binding process was spontaneous, and the negative values of ΔH indicated that the binding was mainly enthalpy-driven and involved an exothermic reaction, the ΔS was unfavorable for it. A positive ΔS value is frequently taken as a typical evidence for hydrophobic interaction, which was consistent with the above discussion. The negative ΔH value (−13.189 kJ/mol) observed cannot be mainly attributed to electrostatic interactions since the ΔH values of electrostatic interactions were very small, almost zero. Therefore, $\Delta H < 0$ and $\Delta S > 0$ obtained in this case indicated that the hydrophobic interactions and hydrogen bonds played an important role in the binding of compound **9a** to HSA, and electrostatic interactions might also involve in the binding process [46].

2.4.5. Effect of common ions

HSA plays a major role in the transport of metal ions in blood plasma, in which Fe^{3+}, K^{+} and Mg^{2+} ions are the major elements present in human body. Other metal ions such as Cu^{2+}, Ca^{2+}, Zn^{2+}, Ni^{2+} and Pb^{2+} ones are considered as trace elements that are indispensable for human health as they have structural and functional roles in many biomolecules. It is reported that metal ions can form complexes with HSA and hence, influence drug binding to HSA. Therefore, the effect of the above metal ions on the binding of compound **9a** to HSA was studied at 298 K (Supplementary information). The competition between the metal ions and compound **9a** led to the binding constants of **9a**–HSA complex ranging from 81.9% to 132.4% of the values of binding constant in absence of metal ions (Table 5). The altered binding constants might be explained by the conformational changes of HSA when bound to metal ions, which in turn affected protein binding to drugs. Clearly, the presence of metal ions such as Cu^{2+}, Ca^{2+}, Zn^{2+}, Ni^{2+} and Pb^{2+} ones decreased the binding constants of **9a**–HSA complex, thereby causing compound **9a** to be quickly cleared from blood, which might lead to more doses of compound **9a** to achieve the desired therapeutic effectiveness. While the participation of Fe^{3+}, K^{+} and Mg^{2+} ions increased the binding constants of **9a**–HSA complex, suggesting the presence of these metal ions could increase the concentration of free compound **9a**, and shorten its the storage time and half-life in the blood, thus improve the maximum efficacy [47].

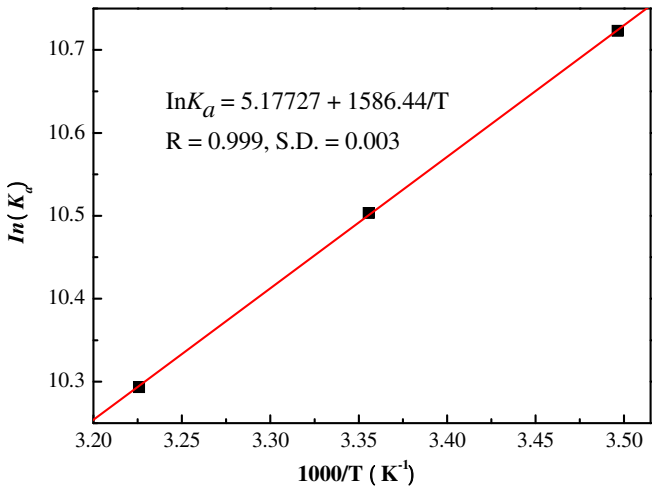

Fig. 12. Van't Hoff plots of the **9a**–HSA system.

Table 4
Thermodynamic parameters of **9a**–HSA system at different temperatures.

T (K)	ΔH (kJ/mol)	ΔG (kJ/mol)	ΔS (J/mol K)
286	−13.189	−25.500	43.044
298		−26.016	
310		−26.533	

3. Conclusion

In conclusion, a series of α-triazolyl chalcones were synthesized through convenient, efficient and economic synthetic procedures. All the target compounds were characterized by ^{1}H NMR, ^{13}C NMR, IR, MS, HRMS spectra. Their *in vitro* antibacterial and antifungal activities indicated that most of the synthesized α-triazolyl chalcones could significantly inhibit the growth of all the tested strains, and some even displayed equipotent or superior activities to the current clinical drugs. Notably, the accidentally obtained compound **9a** gave comparable inhibitory behaviors against MRSA (MIC = 4 μg/mL) and *Bacillus subtilis* (MIC = 8 μg/mL) to chloromycin. The specific interaction of compound **9a** with calf thymus DNA displayed that compound **9a** could intercalate into DNA to form **9a**–DNA complex which might further block DNA replication to exert their powerful antibacterial and antifungal activities. Binding investigations revealed that HSA could generate fluorescent quenching by **9a** as a result of the formation of ground-state **9a**–HSA complex, and the calculated parameters indicated that the binding process was spontaneous. Hydrophobic interactions and hydrogen bonds played an important role in the binding of compound **9a** to HSA, while electrostatic interactions might be also involved in the binding process. Competitive interactions between **9a** and metal ions to HSA suggested that the participation of Fe^{3+}, K^{+} and Mg^{2+} ions in **9a**–HSA system could increase the concentration of free compound **9a**, shorten its storage time and half-life in the blood, and thus improve the maximum antimicrobial efficacies.

4. Experimental protocols

4.1. General methods

Melting points were recorded on X-6 melting point apparatus and uncorrected. TLC analysis was done using pre-coated silica gel plates. FT-IR spectra were carried out on Bruker RFS100/S spectrophotometer (Bio-Rad, Cambridge, MA, USA) using KBr pellets in the400–4000 cm^{-1} range. NMR spectra were recorded on a Bruker AV 300 spectrometer using TMS as an internal standard. The

Table 5
Effect of metal ions on the binding constants of **9a**–HSA complex at 298 K.

Systems	$10^{-4}K_a$ (L/mol)	K_a/K_0^a	R^b	S.D.^{c}
9a–HSA	3.64	1	0.999	0.027
9a–HSA–Ca^{2+}	3.23	0.887	0.998	0.192
9a–HSA–Cu^{2+}	3.49	0.959	0.999	0.073
9a–HSA–Fe^{3+}	4.19	1.151	0.999	0.112
9a–HSA–K^{+}	4.82	1.324	0.997	0.187
9a–HSA–Mg^{2+}	3.89	1.068	0.999	0.116
9a–HSA–Ni^{2+}	3.04	0.835	0.996	0.233
9a–HSA–Pb^{2+}	2.98	0.819	0.999	0.039
9a–HSA–Zn^{2+}	3.34	0.918	0.998	0.044

K_0^a is the binding constant of **9a**–HSA complex in the absence of metal ions; K_a is the binding constants of **9a**–HSA complex with metal ions.
R^b is the correlation coefficient.
S.D.^{c} is standard deviation.

chemical shifts were reported in parts per million (ppm), the coupling constants (*J*) were expressed in hertz (Hz) and signals were described as singlet (s), doublet (d), triplet (t), as well as multiplet (m). The mass spectra were recorded on LCMS-2010A and the high-resolution mass spectra (HRMS) were recorded on an IonSpec FT-ICR mass spectrometer with ESI resource. All fluorescence spectra were recorded at 286, 298, 310 K in the range of 300–450 nm on F-2500 Spectrofluorimeter (Hitachi, Tokyo, Japan) equipped with 1.0 cm quartz cells, the widths of both the excitation and emission slit were set as 2.5 nm, and the excitation wavelength was 295 nm. UV spectra were recorded at room temperature on a TU-2450 spectrophotometer (Puxi Analytic Instrument Ltd. of Beijing, China) equipped with 1.0 cm quartz cells. HAS, Calf thymus DNA and NR were obtained from Sigma–Aldrich (St. Louis, MO, USA). Tris, NaCl, HCl were analytical purity. Sample masses were weighed on a microbalance with a resolution of 0.1 mg. All other chemicals and solvents were commercially available, and used without further purification.

4.1.1. General procedures for the preparation of intermediates (**6a–d**) and (**7a–d**)

The intermediates **6** and **7** were prepared according to the previously reported methods [24].

4.1.2. (Z)-1-(2,4-Dimethylphenyl)-3-phenyl-2-(1H-1,2,4-triazol-1-yl)prop-2-en-1-one (**8a**)

A mixture of intermediate **7a** (1.076 g, 5 mmol) and benzaldehyde (0.743 g, 7 mmol) in the presence of glacial acetic acid (0.08 mL, 1.4 mmol) and piperidine (0.08 mL, 1.4 mmol) as catalyst in toluene (30 mL) was stirred under reflux. After the reaction was completed (monitored by TLC, petroleum ether/ethyl acetate, 3/1, V/V), the solvent was removed under reduced pressure, and the residue was dissolved in dichloromethane (30 mL) and extracted with water (3 × 30 mL). After that, the combined organic phase was dried over anhydrous sodium sulfate and concentrated under reduced pressure. The resulting residue was purified by silica gel column chromatography eluting with petroleum ether/ethyl acetate (10/1–2/1, V/V) to give the pure compound **8a** (697 mg) as yellow solid. Yield: 45.9%; mp: 150–152 °C; IR (KBr) *ν*: 3112, 3041 (Ar–H, =C–H), 2910 (CH_3), 1660 (C=O), 1628 (C=C), 1601, 1565, 1515, 1455, 1438, 1411, 1380, 1124, 1119, 833, 763, 689 cm^{-1}; ^1H NMR ($CDCl_3$, 300 MHz) *δ*: 8.21 (s, 1H, triazole 5-*H*), 8.18 (s, 1H, triazole 3-*H*), 7.44 (s, 1H, Ph-C*H*), 7.41 (d, 1H, chalcone 5′-*H*), 7.34–7.29 (m, 2H, *J* = 9.0 Hz, chalcone 2,6-*H*), 7.26 (m, 1H, chalcone 4-*H*), 7.13–7.07 (m, 2H, *J* = 9.0 Hz, chalcone 3,5-*H*), 2.43 (s, 3H, chalcone 2′-CH_3), 2.39 (s, 3H, chalcone 4′-CH_3) ppm; ^{13}C NMR (75 MHz, $CDCl_3$) *δ*: 196.2 (chalcone *C*=O), 152.5 (triazole 5-*C*), 145.1 (triazole 3-*C*), 141.8 (chalcone 2′-*C*), 141.1 (chalcone 4′-*C*), 135.3 (chalcone 1′,1-*C*), 134.6 (chalcone 6′-*C*), 134.2 (chalcone *α*-*C*), 131.0 (chalcone 3′-*C*), 129.1 (chalcone β-*C*), 128.7 (chalcone 2,6-*C*), 128.3 (chalcone 3,5-*C*), 126.9 (chalcone 4,5′-*C*), 21.2 (chalcone 2′,4′-CH_3) ppm; ESI-MS (*m*/*z*): 304 $[M + H]^+$, 326 $[M + Na]^+$, 342 [M + K]; HRMS (TOF) calcd for $C_{19}H_{17}N_3O$ $[M + H]^+$, 304.1405, found, 304.1408.

4.1.3. (Z)-1-(3,4-Dimethylphenyl)-3-phenyl-2-(1H-1,2,4-triazol-1-yl)prop-2-en-1-one (**8b**)

Compound **8b** (1.151 g) was obtained as yellow solid according to general procedure described for **8a** starting from benzaldehyde (0.849 g, 8 mmol) and compound **7b** (1.291 g, 6 mmol). Yield: 61.3%; mp: 115–116 °C; IR (KBr) *ν*: 3110, 3039 (Ar–H, =C–H), 2915 (CH_3), 1658 (C=O), 1626 (C=C), 1560, 1525, 1444, 1430, 1410, 1377, 1120, 830, 760, 685 cm^{-1}; ^1H NMR (300 MHz, $CDCl_3$) *δ*: 8.26 (s, 1H, triazole 5-*H*), 8.15 (s, 1H, triazole 3-*H*), 7.67 (s, 1H, Ph-C*H*), 7.59–7.56 (d, 2H, *J* = 9.0 Hz, chalcone 2′,6′-*H*), 7.38–7.36 (m, 1H, *J* = 6.0 Hz, chalcone 5′-*H*), 7.32–7.30 (d, 2H, chalcone 2,5-*H*), 7.21 (m, 1H, *J* = 6.0 Hz, chalcone 4-*H*), 6.94–6.92 (d, 2H, *J* = 6.0 Hz, chalcone 3,5-*H*), 2.35 (s, 3H, chalcone 3′-CH_3), 2.33 (s, 3H, chalcone 4′-CH_3) ppm; ^{13}C NMR (75 MHz, $CDCl_3$) *δ*: 189.2 (chalcone *C*=O), 152.5 (triazole 5-*C*), 145.1 (triazole 3-*C*), 141.8 (chalcone 4′-*C*), 139.9 (chalcone 2′-*C*), 136.8 (chalcone 1′-*C*), 135.3 (chalcone 1-*C*), 133.6 (chalcone *α*-*C*), 130.5 (chalcone 5′-*C*), 128.7 (chalcone 2,6,6′-*C*), 128.3 (chalcone 3,5-*C*), 127.4 (chalcone β-*C*), 126.9 (chalcone 4-*C*), 126.6 (chalcone 2′-*C*), 20.4 (chalcone 3′-CH_3), 19.5 (chalcone 4′-CH_3) ppm; ESI-MS (*m*/*z*): 326 $[M + Na]^+$, 304 $[M + H]^+$; HRMS (TOF) calcd for $C_{19}H_{17}N_3O$ $[M + H]^+$, 304.1405, found, 304.1401.

4.1.4. (Z)-1-(4-Chlorophenyl)-3-phenyl-2-(1H-1,2,4-triazol-1-yl) prop-2-en-1-one (**8c**)

Compound **8c** (1.350 g) was obtained as yellow solid according to general procedure described for **8a** starting from benzaldehyde (0.963 g, 9.75 mmol) and compound **7c** (1.084 g, 4.90 mmol). Yield: 89.1%; mp: 110–112 °C; IR (KBr) *ν*: 3043.2 (Ar–H, =C–H), 1659.5 (C=O), 1646.3, 1621.6 (C=C), 1490.6, 825.3 cm^{-1}; ^1H NMR (300 MHz, $CDCl_3$) *δ*: 8.55 (s, 1H, triazole 5-*H*), 8.12 (s, 1H, triazole 3-*H*), 8.03 (s, 1H, Ph-C*H*), 7.86 (d, 2H, *J* = 6.0 Hz, chalcone 2′,6′-*H*), 7.70 (m, 2H, *J* = 3.2 Hz, 6.4 Hz, chalcone 2,6-*H*), 7.54 (m, 2H, chalcone 3,5-*H*), 7.51 (d, 2H, *J* = 6.2 Hz, chalcone 3′,5′-*H*), 7.49 (m, 1H, chalcone 4-*H*) ppm; ^{13}C NMR (75 MHz, $CDCl_3$) *δ*: 192.8 (chalcone *C*=O), 152.5 (triazole 5-*C*), 145.1 (triazole 3-*C*), 140.2 (chalcone 4′-*C*), 135.3 (chalcone 1-*C*), 135.1 (chalcone 1′-*C*), 133.6 (chalcone *α*-*C*), 132.9 (chalcone 2′6′-*C*), 128.7 (chalcone 2,6-*C*), 128.3 (chalcone 3,5-*C*), 128.2 (chalcone 3′,5′-*C*), 127.4 (chalcone β-*C*), 126.9 (chalcone 4-*C*) ppm; ESI-MS (*m*/*z*): 310 $[M + H]^+$, 332 $[M + Na]^+$; HRMS (TOF) calcd for $C_{17}H_{12}ClN_3O$ $[M + H]^+$, 310.0740, found, 310.0746.

4.1.5. (Z)-1,3-Bis(4-chlorophenyl)-2-(1H-1,2,4-triazol-1-yl)prop-2-en-1-one (**8d**)

Compound **8d** (1.050 g) was obtained as yellow solid according to general procedure described for **8a** starting from 4-chlorobenzaldehyde (1.085 g, 7.75 mmol) and compound **7d** (1.004 g, 4.54 mmol). Yield: 67.4%; mp: 119–120 °C; IR (KBr) *ν*: 3045.2 (Ar–H, =C–H), 1665.5 (C=O), 1638.3, 1621.6 (C=C), 1490.6, 830.3 cm^{-1}; ^1H NMR (300 MHz, $CDCl_3$) *δ*: 8.31 (s, 1H, triazole 5-*H*), 8.05 (s, 1H, triazole 3-*H*), 7.85 (d, 2H, *J* = 8.6 Hz, chalcone 2′,6′-*H*), 7.54 (s, 1H, Ph-C*H*), 7.35 (d, 2H, *J* = 8.6 Hz, chalcone, 3′,5′-*H*), 7.18 (s, 4H, chalcone 2,3,5,6-*H*) ppm; ^{13}C NMR (75 MHz, $CDCl_3$) *δ*: 190.0 (chalcone *C*=O), 152.5 (triazole 5-*C*), 142.3 (triazole 3-*C*), 141.5 (chalcone 4′-*C*), 135.4 (chalcone 1′-*C*), 133.2 (chalcone 4-*C*), 131.7 (chalcone *α*,1-*C*), 130.9 (chalcone 2′6′-*C*), 130.3 (chalcone 2,6-*C*), 129.5 (chalcone 3,5-*C*), 129.0 (chalcone 3′,5′-*C*), 124.5 (chalcone β-*C*) ppm; ESI-MS (*m*/*z*): 344 $[M + H]^+$, 366 $[M + Na]^+$; HRMS (TOF) calcd for $C_{17}H_{11}Cl_2N_3O$ $[M + H]^+$, 344.0340, found, 344.0341.

4.1.6. (Z)-1-(2,4-Difluorophenyl)-3-phenyl-2-(1H-1,2,4-triazol-1-yl) prop-2-en-1-one (**8e**)

Compound **8e** (2.210 g) was obtained as white solid according to general procedure described for **8a** starting from benzaldehyde (1.060 g, 10 mmol) and compound **7d** (2.230 g, 10 mmol). Yield: 71.0%; mp: 124–125 °C; IR (KBr) *ν*: 3114, 3041 (Ar–H, =C–H), 1654 (C=O), 1633 (C=C), 1604, 1575, 1505, 1465, 1448, 1401, 1134, 1109, 813, 753, 693 cm^{-1}; ^1H NMR (300 MHz, $CDCl_3$) *δ*: 8.16 (s, 2H, triazole 3,5-*H*), 7.64 (t, 1H, *J* = 7.5 Hz, chalcone 6′-*H*), 7.59 (s, 1H, C=C*H*), 7.40 (t, 1H, *J* = 7.5 Hz, chalcone 5′-*H*), 7.31 (t, 2H, *J* = 7.5 Hz, chalcone 2,6-*H*), 7.02 (t, *J* = 7.5 Hz, 1H, chalcone 3′-*H*), 6.93–6.86 (m, 3H, chalcone 3,4,5-*H*) ppm; ^{13}C NMR (75 MHz, $CDCl_3$) *δ*: 187.1 (chalcone *C*=O), 166.9, 166.7, 163.6, 163.3 (chalcone 4′-*C*), 162.2, 158.9, 158.7 (chalcone 2′-*C*), 152.9 (triazole 5-*C*), 145.2 (triazole 3-*C*), 141.8 (chalcone *α*-*C*), 133.1 (chalcone β-*C*), 132.4, 132.2 (chalcone 6′-*C*), 131.8 (chalcone 1-*C*), 130.8 (chalcone 4-*C*), 130.4 (chalcone 2,6-*C*), 129.2 (chalcone 3,5-*C*), 122.1, 121.7 (chalcone 1′-*C*), 112.6, 112.3 (chalcone 5′-*C*),

105.3, 104.5 (chalcone 3′-*C*) ppm; ESI-MS (*m/z*): 312 $[M + H]^+$, 274 $[M + H - 2F]^+$; ESI-MS (*m/z*): 312 $[M + H]^+$, 334 $[M + Na]^+$; HRMS (TOF) calcd for $C_{17}H_{11}F_2N_3O$ $[M + H]^+$, 312.0940, found, 312.0946.

4.1.7. (Z)-3-(4-Chlorophenyl)-1-(2,4-difluorophenyl)-2-(1H-1,2,4-triazol-1-yl)prop-2-en-1-one (**8f**)

Compound **8f** (2.610 g) was obtained as yellow solid according to general procedure described for **8a** starting from 4-chlorobenzaldehyde (1.410 g, 10 mmol) and compound **7d** (2.230 g, 10 mmol). Yield: 75.6%; mp: 102–104 °C; IR (KBr) *ν*: 3033.2 (Ar–H, =C–H), 1662.5 (C=O), 1636.3 (C=C), 1611.6, 1499.6, 820.3 cm^{-1}; ^1H NMR (300 MHz, $CDCl_3$) *δ*: 8.16 (s, 2H, triazole 3,5-*H*), 7.66 (dd, *J* = 14.8 Hz, 7.7 Hz, 1H, chalcone 3′-*H*), 7.54 (s, 1H, C=C*H*), 7.31–7.28 (d, *J* = 8.7 Hz, 2H, chalcone 2,6-*H*), 7.04 (t, *J* = 8.0 Hz, 1H, chalcone 5′-*H*), 6.93 (d, *J* = 8.0 Hz, 1H, chalcone 6′-*H*), 6.87 (d, *J* = 8.0 Hz, 2H, chalcone 3,5-*H*). ppm; ^{13}C NMR (75 MHz, $CDCl_3$) *δ*: 186.8 (chalcone *C*=O), 166.8, 163.6 (chalcone 4′-*C*), 162.2, 158.6 (chalcone 2′-*C*), 152.9 (triazole 5-*C*), 145.2 (triazole 3-*C*), 140.2 (chalcone 6′-*C*), 138.0 (chalcone α-*C*), 133.3 (chalcone 4-*C*), 132.3 (chalcone 1-*C*), 131.5 (chalcone 2,6-*C*), 129.5 (chalcone 3,5-*C*), 129.2 (chalcone β-*C*), 121.7, 121.5 (chalcone 1′-*C*), 112.6 (chalcone 5′-*C*), 105.1, 104.8, 104.5 (chalcone 3′-*C*) ppm; ESI-MS (*m/z*): 346 $[M + H]^+$, 368 $[M + Na]^+$; HRMS (TOF) calcd for $C_{17}H_{10}N_3OClF_2$ $[M + H]^+$, 346.0552; found, 346.0553.

4.1.8. (Z)-1-(2,4-Difluorophenyl)-3-(4-fluorophenyl)-2-(1H-1,2,4-triazol-1-yl)prop-2-en-1-one (**8g**)

Compound **8g** (4.050 g) was obtained as white solid according to general procedure described for **8a** starting from 4-fluorobenzaldehyde (1.896 g, 15.29 mmol) and compound **7d** (3.069 g, 13.76 mmol). Yield: 89.4%; mp: 113–115 °C; IR (KBr) *ν*: 3030.2 (Ar–H, =C–H), 1660.5 (C=O), 1630.3(C=C), 1621.6, 1495.6, 825.3 cm^{-1}; ^1H NMR (300 MHz, $CDCl_3$) *δ*: 8.17 (s, 2H, triazole 3,5-*H*), 7.64 (dd, *J* = 14.8 Hz, 7.7 Hz, 1H, chalcone 3′-*H*), 7.55 (s, 1H, C=C*H*), 7.05 (d, *J* = 8.7 Hz, 2H, chalcone 2,6-*H*), 6.98 (t, *J* = 8.0 Hz, 1H, chalcone 5′-*H*), 6.92 (d, *J* = 8.0 Hz, 1H, chalcone 6′-*H*), 6.89 (d, *J* = 8.0 Hz, 2H, chalcone 3,5-*H*). ppm; ^{13}C NMR (75 MHz, $CDCl_3$) *δ*: 186.9 (chalcone *C*=O), 166.9, 163.4 (chalcone 4′-*C*), 166.1 (triazole 5-*C*), 163.4, 161.9 (chalcone 2′-*C*), 162.7 (triazole 3-*C*), 152.9 (chalcone 4-*C*), 145.2 (chalcone 6′-*C*), 140.6 (chalcone α-*C*), 132.2 (chalcone 2,6-*C*), 132.1 (chalcone 1-*C*), 127.0 (chalcone β-*C*), 121.6 (chalcone 1′-*C*), 116.7 (chalcone 3,5-*C*), 112.6, 112.3 (chalcone 5′-*C*), 105.1, 104.8, 104.5 (chalcone 3′-*C*) ppm; HRMS (TOF) calcd for $C_{17}H_{10}N_3OF_3$ $[M + H]^+$, 330.0854, found, 330.0849.

4.1.9. (Z)-1-(2,4-Difluorophenyl)-3-(4-methylphenyl)-2-(1H-1,2,4-triazol-1-yl)prop-2-en-1-one (**8h**)

Compound **8h** (1.256 g) was obtained as white solid according to general procedure described for **8a** starting from 4-methylbenzaldehyde (0.963 g, 8.02 mmol) and compound **7d** (1.084 g, 4.89 mmol). Yield: 79.0%; mp: 105–106 °C; IR (KBr) *ν*: 3105.8 (Ar–H, =C–H), 2960.1, 2830.5 (CH_3), 1665.5 (C=O), 1600.1, 1517.3, 1461.2, 830.4 cm^{-1}; ^1H NMR (300 MHz, $CDCl_3$) *δ*: 8.16 (d, *J* = 5.2 Hz, 2H, triazole 3,5-*H*), 7.63 (dd, *J* = 14.6 Hz, 8.2 Hz, 1H, chalcone 3′-*H*), 7.56 (s, 1H, Ph-C*H*), 7.10 (d, *J* = 8.0 Hz, 2H, chalcone 2,6-*H*), 7.01 (t, *J* = 7.2 Hz, 1H, chalcone 6′-*H*), 6.92–6.83 (m, 1H, chalcone 5′-*H*), 6.78 (d, *J* = 8.1 Hz, 2H, chalcone 3,5-*H*), 2.34 (s, 3H, chalcone 4-C*H*$_3$). ppm; ^{13}C NMR (75 MHz, $CDCl_3$) *δ*: 187.1 (chalcone *C*=O), 166.8, 163.4 (chalcone 4′-*C*), 162.1, 158.7 (chalcone 2′-*C*), 152.9 (triazole 5-*C*), 145.2 (triazole 3-*C*), 142.9 (chalcone 4-*C*), 142.6 (chalcone 6′-*C*), 132.4 (chalcone α-*C*), 131.9 (chalcone 1-*C*), 130.6 (chalcone 2,6-*C*), 129.9 (chalcone 3,5-*C*), 127.9 (chalcone β-*C*), 122.0 (chalcone 1′-*C*), 112.4 (chalcone 5′-*C*), 105.1, 104.8, 104.5 (chalcone 3′-*C*), 21.6 (chalcone 4-*C*H$_3$) ppm; ESI-MS (*m/z*): 326 $[M + H]^+$, 348 $[M + Na]^+$; HRMS (TOF) calcd for $C_{18}H_{13}N_3OF_2$ $[M + H]^+$, 326.1054; found, 326.1049.

4.1.10. (Z)-1-(2,4-Difluorophenyl)-3-(4-methoxyphenyl)-2-(1H-1,2,4-triazol-1-yl)prop-2-en-1-one (**8i**)

Compound **8i** (2.600 g) was obtained as yellow solid according to general procedure described for **8a** starting from 4-methoxylbenzaldehyde (1.360 g, 10 mmol) and compound **7d** (2.230 g, 10 mmol). Yield: 76.2%; mp: 144–145 °C; IR (KBr) *ν*: 3055.8 (Ar–H, =C–H), 2966.1, 2839.5 (CH_3), 1660.5 (C=O), 1606.1 (C=C), 1507.3, 1460.2, 833.4 (=C–H) cm^{-1}; ^1H NMR (300 MHz, $CDCl_3$) *δ*: 8.20 (d, *J* = 3.1 Hz, 2H, triazole 3,5-*H*), 7.62 (dd, *J* = 14.6 Hz, 8.2 Hz, 1H, chalcone 3′-*H*), 7.56 (s, 1H, Ph-C*H*), 7.02 (t, *J* = 8.2 Hz, 1H, chalcone 6′-*H*), 6.95–6.86 (m, 1H, chalcone 5′-*H*), 6.82 (s, 4H, chalcone 2,3,5,6-*H*), 3.82 (s, 3H, chalcone 4-C*H*$_3$) ppm; ^{13}C NMR (75 MHz, $CDCl_3$) *δ*: 187.0 (chalcone *C*=O), 166.5, 163.2 (chalcone 4′-*C*), 162.7 (chalcone 4-*C*), 161.9, 158.5 (chalcone 2′-*C*), 152.9 (triazole 5-*C*), 145.2 (triazole 3-*C*), 142.9 (chalcone 6′-*C*), 132.9 (chalcone 2,6-*C*), 132.0 (chalcone α-*C*), 130.8 (chalcone β-*C*), 123.2 (chalcone 1-*C*), 114.7 (chalcone 3,5-*C*), 122.1 (chalcone 1′-*C*), 112.4, 112.1 (chalcone 5′-*C*), 105.1, 104.7, 104.4 (chalcone 3′-*C*), 55.4 (chalcone 4-OCH_3) ppm; ESI-MS (*m/z*): 342 $[M + H]^+$, 364 $[M + Na]^+$; HRMS (TOF) calcd for $C_{18}H_{13}N_3O_2F_2$ $[M + H]^+$, 342.1054; found, 342.1049.

4.1.11. (Z)-1-(2,4-Difluorophenyl)-3-(4-(dimethylamino)phenyl)-2-(1H-1,2,4-triazol-1-yl)prop-2-en-1-one (**8j**)

Compound **8j** (2.809 g) was obtained as yellow solid according to general procedure described for **8a** starting from 4-(dimethylamino)benzaldehyde (1.408 g, 10 mmol) and compound **7d** (2.230 g, 10 mmol). Yield: 79.3%; mp: 131–133 °C; IR (KBr) *ν*: 3126.7 (Ar–H, =C–H), 2929.1 (CH_3), 1655.5 (C=O), 1600.1, 1512.4, 1466.2 cm^{-1}; ^1H NMR (300 MHz, $CDCl_3$) *δ*: 8.55 (s, 1H, triazole 5-*H*), 8.12 (s, 1H, triazole 3-*H*), 8.03 (s, 1H, C=C*H*), 7.92 (d, 2H, *J* = 15.0 Hz, chalcone 2,6-*H*), 7.73 (m, 1H, chalcone 6′-*H*), 7.25 (m, 1H, *J* = 2.7 Hz, 13.8 Hz, chalcone 5′-*H*), 7.04 (m, 1H, chalcone 3′-*H*), 6.99 (d, 2H, *J* = 15.0 Hz, chalcone 3,5-*H*), 3.02 (s, 6H, chalcone 4-N(CH_3)$_2$) ppm; ^{13}C NMR (75 MHz, $CDCl_3$) *δ*: 191.0 (chalcone *C*=O), 170.1, 167.8 (chalcone 4′-*C*), 166.7, 164.4 (chalcone 2′-*C*), 152.5 (triazole 5-*C*), 152.0 (chalcone 4-*C*), 145.1 (triazole 3-*C*), 135.5 (chalcone 6′-*C*), 134.2 (chalcone α-*C*), 129.5 (chalcone 2,6-*C*), 129.1 (chalcone β-*C*), 122.7 (chalcone 1-*C*), 121.2 (chalcone 1′-*C*), 115.9 (chalcone 5′-*C*), 113.3 (chalcone 3,5-*C*), 109.6 (chalcone 3′-*C*), 41.9 (chalcone 4-NCH_3) ppm; ESI-MS (*m/z*): 355 $[M + H]^+$, 377 $[M + Na]^+$; HRMS (TOF) calcd for $C_{19}H_{16}N_4OF_2$ $[M + H]^+$, 355.1365; found, 355.1363.

4.1.12. General procedure for "one-pot" preparation of α-triazolyl mono-aminochalcone hybrids (**9a**–**c**) and α-triazolyl bis-aminochalcone hybrids (**10a**–**c**)

A mixture of intermediate **7d** (2.230 g, 10 mmol), benzaldehyde (1.060 g, 10 mmol) and cyclic amine (20 mmol) in the presence of acetic acid (0.08 mL, 1.4 mmol) as catalyst in toluene (30 mL) was stirred under reflux. After the reaction was completed (monitored by TLC, petroleum ether/ethyl acetate, 3/1, V/V), the solvent was removed under reduced pressure, and the residue was dissolved in dichloromethane (30 mL) and extracted with water (3 × 30 mL). After that, the combined organic phase was dried over anhydrous sodium sulfate and concentrated under reduced pressure to give the crude material, which was purified by silica gel column chromatography eluting with petroleum ether/ethyl acetate (15/1–1/1, V/V) to afford the desired α-triazolyl mono-aminochalcone hybrids (**9a**–**c**) and α-triazolyl bis-aminochalcone hybrids (**10a**–**c**) simultaneously.

4.1.13. (Z)-1-(4-Fluoro-2-(piperidin-1-yl)phenyl)-3-phenyl-2-(1H-1,2,4-triazol-1-yl) prop-2-en-1-one (**9a**)

Compound **9a** (2.010 g) was obtained as yellow solid according to the general procedure described for **9a**–**c** starting from piperidine (1.700 g, 20 mmol), compound **7d** (2.230 g, 10 mmol) and

benzaldehyde (1.060 g, 10 mmol). Yield: 53.4%; mp: 135–136 °C; IR (KBr) ν: 3110, 3078 (Ar–H, =C–H), 2976 (CH_2), 1653 (C=O), 1634, 1596, 1503, 1454, 1401, 1242, 1165, 1128, 866, 768, 692 cm^{-1}; ^1H NMR (300 MHz, $CDCl_3$) δ: 8.09 (s, 1H, triazole 5-*H*), 8.07 (s, 1H, triazole 3-*H*), 7.56 (s, 1H, C=C*H*), 7.46–7.28 (m, 4H, chalcone 6′,2,4,6-*H*), 6.88 (d, 2H, J = 9.0 Hz, chalcone 3,5-*H*), 6.77 (t, 1H, J = 9.0 Hz, chalcone 3′-*H*), 6.71–6.67 (m, 1H, chalcone 5′-*H*), 2.95 (s, 4H, piperidyl 2,6-*H*), 1.64 (s, 4H, piperidyl 3,5-*H*), 1.52 (s, 2H, piperidyl 4-*H*) ppm; ^{13}C NMR (75 MHz, $CDCl_3$) δ: 192.5 (chalcone *C*=O), 166.8, 163.5 (chalcone 4′-*C*), 154.1, 154.0 (chalcone 2′-*C*), 152.3 (triazole 5-*C*), 145.1 (triazole 3-*C*), 140.4 (chalcone 1-*C*), 132.4 (chalcone α-*C*), 132.3, 132.2 (chalcone 6′-*C*), 131.3 (chalcone β-*C*), 131.2 (chalcone 4-*C*), 130.0 (chalcone 2,6-*C*), 129.1 (chalcone 3,5-*C*), 127.4, 127.3 (chalcone 1′-*C*), 109.0, 108.7 (chalcone 5′-*C*), 105.8, 105.5 (chalcone 3′-*C*), 53.8 (piperidyl 2,6-*C*), 25.9 (piperidyl 3,5-*C*), 23.8 (piperidyl 4-*C*) ppm; ESI-MS (m/z): 399 $[M + Na]^+$, 377 $[M + H]^+$, 274 $[M + H - F -$ piperidyl$]^+$; HRMS (TOF) calcd for $C_{22}H_{21}FN_4O$ $[M + H]^+$, 377.1769; found, 377.1774.

4.1.14. (Z)-1-(4-Fluoro-2-(morpholin-4-yl)phenyl)-3-phenyl-2-(1H-1,2,4-triazol-1-yl)prop-2-en-1-one (**9b**)

Compound **9b** (2.090 g) was obtained as yellow solid according to the general procedure described for **9a**–**c** starting from morpholine (1.740 g, 20 mmol), compound **7d** (2.230 g, 10 mmol) and benzaldehyde (1.060 g, 10 mmol). Yield: 55.3%; mp: 123–124 °C; IR (KBr) ν: 3130, 3060 (Ar–H, =C–H), 2970, 2855 (CH_2), 1655 (C=O), 1640, 1601 (C=C), 1573, 1498, 1299, 1109, 987, 881, 774, 617 cm^{-1}; ^1H NMR (300 MHz, $CDCl_3$) δ: 8.11 (s, 1H, triazole 5-*H*), 8.06 (s, 1H, triazole 3-*H*), 7.49 (s, 1H, C=C*H*), 7.48–7.30 (m, 4H, chalcone 6′,2,4,6-*H*), 6.88–6.86 (m, 3H, chalcone 3,5,3′-*H*), 6.74–6.69 (m, 1H, chalcone 5′-*H*), 3.75 (t, 4H, J = 4.2 Hz, morpholinyl OCH_2), 2.99 (t, 4H, J = 4.5 Hz, morpholinyl NCH_2) ppm; ^{13}C NMR (75 MHz, $CDCl_3$) δ: 192.4 (chalcone *C*=O), 166.8, 163.6 (chalcone 4′-*C*), 153.1, 153.0 (chalcone 2′-*C*), 152.5 (triazole 5-*C*), 145.1 (triazole 3-*C*), 141.0 (chalcone 1-*C*), 132.6 (chalcone α-*C*), 132.4, 132.3 (chalcone 6′-*C*), 131.4 (chalcone β-*C*), 131.1 (chalcone 4-*C*), 130.0 (chalcone 2,6-*C*), 129.2 (chalcone 3,5-*C*), 127.2, 127.1 (chalcone 1′-*C*), 109.9, 109.6 (chalcone 5′-*C*), 105.9, 105.5 (chalcone 3′-*C*), 66.6 (morpholinyl OCH_2), 52.5 (morpholinyl NCH_2) ppm; ESI-MS (m/z): 379 $[M + H]^+$, 274 $[M + H - F -$ morpholinyl$]^+$; HRMS-TOF: m/z $[M + H]^+$ calcd for $C_{21}H_{19}FN_4O_2$: 379.1504, found: 379.1501.

4.1.15. (Z)-1-(4-Fluoro-2-(pyrrolidin-1-yl)phenyl)-3-phenyl-2-(1H-1,2,4-triazol-1-yl) prop-2-en-1-one (**9c**)

Compound **9c** (0.830 g) was obtained as yellow solid according to the general procedure described for **9a**–**c** starting from pyrrolidine (1.420 g, 20 mmol), compound **7d** (2.230 g, 10 mmol) and benzaldehyde (1.060 g, 10 mmol). Yield: 23.1%; mp: 150–152 °C; IR (KBr) ν: 3114, 3040 (Ar–H, =C–H), 2929, 2852 (CH_2), 1663 (C=O), 1592 (C=C), 1502, 1399, 1109, 856, 752, 638 cm^{-1}; ^1H NMR (300 MHz, $CDCl_3$) δ: 8.17 (s, 1H, triazole 5-*H*), 8.16 (s, 1H, triazole 3-*H*), 7.64 (s, 1H, C=C*H*), 7.50–7.45 (m, 1H, chalcone 6′-*H*), 7.37–7.28 (m, 3H, chalcone 2,4,6-*H*), 6.89 (d, 2H, J = 6.0 Hz, chalcone 3,5-*H*), 6.50–6.40 (m, 2H, chalcone 3′,5′-*H*), 3.21 (t, 4H, J = 6.3 Hz, pyrrolidyl 2,5-*H*), 1.98 (t, 4H, J = 6.3 Hz, pyrrolidyl 3,4-*H*) ppm; ^{13}C NMR (75 MHz, $CDCl_3$) δ: 180.7 (chalcone *C*=O), 167.0, 163.7 (chalcone 4′-*C*), 152.5 (triazole 5-*C*), 150.0, 149.8 (chalcone 2′-*C*), 145.1 (triazole 3-*C*), 141.6 (chalcone 1-*C*), 133.5 (chalcone α-*C*), 133.2, 133.1 (chalcone 6′-*C*), 131.3 (chalcone β-*C*), 131.1 (chalcone 4-*C*), 130.2 (chalcone 2,6-*C*), 129.0 (chalcone 3,5-*C*), 118.3 (chalcone 1′-*C*), 102.8, 102.5 (chalcone 5′-*C*), 100.7, 100.4 (chalcone 3′-*C*), 51.2 (pyrrolidyl 2,5-*C*), 25.9 (pyrrolidyl 3,6-*C*) ppm; ESI-MS (m/z): 363 $[M + H]^+$, 274 $[M + H - F -$ pyrrolidyl$]^+$; HRMS (TOF) calcd for $C_{21}H_{19}FN_4O$ $[M + H]^+$, 362.1509; found, 362.1505.

4.1.16. (Z)-1-(2,4-Di(piperidin-1-yl)phenyl)-3-phenyl-2-(1H-1,2,4-triazol-1-yl) prop-2-en-1-one (**10a**)

Compound **10a** (0.750 g) was obtained as red syrup according to the general procedure described for **10a**–**c** starting from piperidine (1.700 g, 20 mmol), compound **7d** (2.230 g, 10 mmol) and benzaldehyde (1.060 g, 10 mmol). Yield: 17.0%; IR (KBr) ν: 3125, 3075 (Ar–H, =C–H), 2964, 2858 (CH_2), 1665 (C=O), 1612, 1573, 1552 (C=C), 1449, 1231, 1201, 1057, 951, 818, 617 cm^{-1}; ^1H NMR (300 MHz, $CDCl_3$) δ: 8.08 (s, 2H, triazole 3,5-*H*), 7.51 (s, 1H, C=C*H*), 7.43 (d, 1H, J = 9.2 Hz, chalcone 6′-*H*), 7.33–7.29 (m, 3H, chalcone 2,4,6-*H*), 6.88 (d, 2H, J = 9.2 Hz, chalcone 3,5-*H*), 6.56 (d, 1H, J = 6.0 Hz, chalcone 5′-*H*), 6.40 (s, 1H, chalcone 3′-*H*), 3.29–3.27 (m, 4H, 2′-piperidyl 2,6-*H*), 2.94–2.92 (m, 4H, 4′-piperidyl 2,6-*H*), 1.69–1.61 (m, 12H, piperidyl 3,4,5-*H*) ppm; ^{13}C NMR (75 MHz, $CDCl_3$) δ: 192.1 (chalcone *C*=O), 154.9 (chalcone 2′-*C*), 154.3 (chalcone 4′-*C*), 152.1 (triazole 5-*C*), 145.2 (triazole 3-*C*), 139.0 (chalcone 6′-*C*), 133.1 (chalcone 1-*C*), 132.8 (chalcone α-*C*), 131.9 (chalcone β-*C*), 130.5 (chalcone 4-*C*), 129.8 (chalcone 2,6-*C*), 128.9 (chalcone 3,5-*C*), 120.7 (chalcone 1′-*C*), 108.3 (chalcone 5′-*C*), 104.2 (chalcone 3′-*C*), 54.0 (2′-piperidyl 2,6-*C*), 49.1 (4′-piperidyl 2,6-*C*), 26.0 (2′-piperidyl 3,5-*C*), 25.5 (4′-piperidyl 3,5-*C*), 24.3 (2′-piperidyl 4-*C*), 24.1 (4′-piperidyl 4-*C*) ppm; ESI-MS (m/z): 442 $[M + H]^+$; HRMS (TOF) calcd for $C_{27}H_{31}N_5O$ $[M + H]^+$, 442.2599; found, 442.2601.

4.1.17. (Z)-1-(2,4-Di(morpholin-4-yl)phenyl)-3-phenyl-2-(1H-1,2,4-triazol-1-yl)prop-2-en-1-one (**10b**)

Compound **10b** (0.851 g) was obtained as red syrup according to the general procedure described for **10a**–**c** starting from morpholine (1.740 g, 20 mmol), compound **7d** (2.230 g, 10 mmol) and benzaldehyde (1.060 g, 10 mmol). Yield: 19.1%; IR (KBr) ν: 3116 (Ar–H, =C–H), 2840 (CH_2), 1632 (C=O), 1506, 1400, 1131, 1109, 617 cm^{-1}; ^1H NMR (300 MHz, $CDCl_3$) δ: 8.10 (s, 1H, triazole 5-*H*), 8.05 (s, 1H, triazole 3-*H*), 7.49 (s, 1H, C=C*H*), 7.46 (s, 1H, chalcone 6′-*H*), 7.35–7.28 (m, 3H, chalcone 2,4,6-*H*), 6.88 (d, 2H, J = 9.2 Hz, chalcone 3,5-*H*), 6.63–6.60 (m, 1H, chalcone 5′-*H*), 6.42 (s, 1H, chalcone 3′-*H*), 3.87 (t, 4H, J = 4.5 Hz, 2′-morpholinyl OCH_2), 3.75 (t, 4H, J = 4.5 Hz, 4′-morpholinyl OCH_2), 3.28 (t, 4H, J = 4.5 Hz, 2′-morpholinyl NCH_2), 3.00 (t, 4H, J = 4.5 Hz, 4′-morpholinyl NCH_2) ppm; ^{13}C NMR (75 MHz, $CDCl_3$) δ: 191.8 (chalcone *C*=O), 169.2 (chalcone 2′-*C*), 154.6 (chalcone 4′-*C*), 153.1 (triazole 5-*C*), 152.3 (chalcone 6′-*C*), 145.2 (triazole 3-*C*), 139.7 (chalcone 1-*C*), 132.9 (chalcone α-*C*), 131.5 (chalcone β-*C*), 130.9 (chalcone 4-*C*), 129.9 (chalcone 2,6-*C*), 129.1 (chalcone 3,5-*C*), 121.4 (chalcone 1′-*C*), 108.5 (chalcone 5′-*C*), 103.5 (chalcone 3′-*C*), 66.8 (2′-morpholinyl OCH_2), 66.6 (4′-morpholinyl OCH_2), 47.9 (2′-morpholinyl NCH_2), 46.6 (4′-morpholinyl NCH_2) ppm; ESI-MS (m/z): 468 $[M + Na]^+$, 446 $[M + H]^+$; HRMS (TOF) calcd for $C_{25}H_{27}N_5O_3$ $[M + H]^+$, 446.5144; found, 446.5141.

4.1.18. (Z)-1-(2,4-Di(pyrrolidin-1-yl)phenyl)-3-phenyl-2-(1H-1,2,4-triazol-1-yl)prop -2-en-1-one (**10c**)

Compound **10c** (0.530 g) was obtained as red syrup according to the general procedure described for **10a**–**c** starting from pyrrolidine (1.420 g, 20 mmol), compound **7d** (2.230 g, 10 mmol) and benzaldehyde (1.060 g, 10 mmol). Yield: 13.1%; IR (KBr) ν: 3103 (Ar–H, =C–H), 2964, 2868 (CH_2), 1668 (C=O), 1600, 1501 (C=C), 1448, 1397, 1132, 1110, 797, 696, 638 cm^{-1}; ^1H NMR (300 MHz, $CDCl_3$) δ: 8.20 (s, 1H, triazole 5-*H*), 8.14 (s, 1H, triazole 3-*H*), 7.56 (s, 1H, C=C*H*), 7.54 (s, 1H, chalcone 6′-*H*), 7.32–7.28 (m, 3H, chalcone 2,4,6-*H*), 6.90 (d, 2H, J = 6.0 Hz, chalcone 3,5-*H*), 6.02–5.99 (m, 1H, chalcone 5′-*H*), 5.80 (d, 1H, J = 3.0 Hz, chalcone 3′-*H*), 3.35 (t, 4H, J = 7.5 Hz, 2′-pyrrolidyl 2,5-*H*), 3.25 (t, 4H, J = 6.0 Hz, 4′-pyrrolidyl 2,5-*H*), 2.02–1.95 (m, 8H, pyrroly 3,4-*H*) ppm; ^{13}C NMR (75 MHz, $CDCl_3$) δ: 187.7 (chalcone *C*=O), 152.2 (chalcone 2′-*C*), 151.1 (chalcone 4′-*C*), 150.8 (triazole 5-*C*), 145.1 (triazole 3-*C*), 137.9 (chalcone 6′-*C*), 134.4 (chalcone 1-*C*), 134.2 (chalcone α-*C*), 131.9 (chalcone β-*C*), 130.3

(chalcone 4-*C*), 129.8 (chalcone 2,6-*C*), 128.8 (chalcone 3,5-*C*), 111.9 (chalcone 1′-*C*), 101.1 (chalcone 5′-*C*), 94.9 (chalcone 3′-*C*), 51.4 (2′-pyrrolidyl 2,5-*C*), 47.5 (4′-pyrrolidyl 2,5-*C*), 25.9 (2′-pyrrolidyl 3,6-*C*), 25.4 (4′-pyrrolidyl 3,6-*C*) ppm; ESI-MS (*m*/*z*): 414 $[M + H]^+$, 274 $[M + H-2$ pyrrolidyl$]^+$; HRMS (TOF) calcd for $C_{25}H_{27}N_5O$ $[M + H]^+$, 414.2216; found, 414.2210.

Acknowledgments

This work was partially supported by National Natural Science Foundation of China [(No. 21172181, 21372186), the Research Fund for International Young Scientists from International (Regional) Cooperation and Exchange Program (No. 81350110338, 81250110554)], the Key Program of Natural Science Foundation of Chongqing (CSTC2012jjB10026), the Specialized Research Fund for the Doctoral Program of Higher Education of China (SRFDP 20110182110007).

Appendix A. Supplementary data

Supplementary data related to this article can be found at http://dx.doi.org/10.1016/j.ejmech.2013.11.003.

References

[1] X. Jin, C.J. Zheng, M.X. Song, Y. Wu, L.P. Sun, Y.J. Li, L.J. Yu, H.R. Piao, Eur. J. Med. Chem. 56 (2012) 203–209.
[2] X.M. Peng, G.X. Cai, C.H. Zhou, Curr. Top. Med. Chem. 13 (2013) 1963–2010.
[3] L. Zhang, X.M. Peng, G.L.V. Damu, R.X. Geng, C.H. Zhou. Med. Res. Rev., http://dx.doi.org/10.1002/med.21290.
[4] R. Schobert, B. Biersack, A. Dietrich, S. Knauer, M. Zoldakova, A. Fruehauf, T. Mueller, J. Med. Chem. 52 (2009) 241–246.
[5] S. Vogel, M. Barbic, G. Jürgenliemk, J. Heilmann, Eur. J. Med. Chem. 45 (2010) 2206–2213.
[6] N. Zhang, Z.W. Liu, Q.Y. Han, J.H. Chen, Y. Lv, Phytomedicine 17 (2010) 310–316.
[7] V. Tomar, G. Bhattacharjee, S. Rajakumar, Kamaluddin, K. Srivastava, S.K. Puri, Eur. J. Med. Chem. 45 (2010) 745–751.
[8] J.C. Aponte, D. Castillo, Y. Estevez, G. Gonzalez, J. Arevalo, G.B. Hammond, M. Sauvain, Bioorg. Med. Chem. Lett. 20 (2010) 100–103.
[9] R.G. Damazio, A.P. Zanatta, L.H. Cazarolli, A. Mascarello, L.D. Chiaradia, R.J. Nunes, R.A. Yunes, F.R.M.B. Silva, Biochimie 91 (2009) 1493–1498.
[10] A. Solankee, K. Kapadia, A. Ćiric, M. Sokovic, I. Doytchinova, A. Geronikaki, Eur. J. Med. Chem. 45 (2010) 510–518.
[11] Z. Nowakowska, Eur. J. Med. Chem. 42 (2007) 125–137.
[12] N. Tadigoppula, V. Korthikunta, S. Gupta, P. Kancharla, T. Khaliq, A. Soni, R.K. Srivastava, K. Srivastava, S.K. Puri, K.S.R. Raju, Wahajuddin, P.S. Sijwali, V. Kumar, I.S. Mohammad, J. Med. Chem. 56 (2013) 31–45.
[13] N. Selvakumar, G.S. Kumar, A.M. Azhagan, G.G. Rajulu, S. Sharma, M.S. Kumar, J. Das, J. Iqbal, S. Trehan, Eur. J. Med. Chem. 42 (2007) 538–543.
[14] X.F. Liu, C.J. Zheng, L.P. Sun, X.K. Liu, H.R. Piao, Eur. J. Med. Chem. 46 (2011) 3469–3473.
[15] T. Hussain, H.L. Siddiqui, M. Zia-ur-Rehman, M.M. Yasinzai, M. Parvez, Eur. J. Med. Chem. 44 (2009) 4654–4660.
[16] X.M. Peng, G.L.V. Damu, C.H. Zhou, Curr. Pharm. Des. 19 (2013) 3884–3930.
[17] N. Anand, P. Singh, A. Sharma, S. Tiwari, V. Singh, D.K. Singh, K.K. Srivastava, B.N. Singh, R.P. Tripathi, Bioorg. Med. Chem. 20 (2012) 5150–5163.
[18] C.H. Zhou, Y. Wang, Curr. Med. Chem. 19 (2012) 239–280.
[19] C.Q. Sheng, W.N. Zhang, H.T. Ji, M. Zhang, Y.L. Song, H. Xu, J. Zhu, Z.Y. Miao, Q.F. Jiang, J.Z. Yao, Y.J. Zhou, J. Zhu, J.G. Lu, J. Med. Chem. 49 (2006) 2512–2525.
[20] H.Z. Zhang, G.L.V. Damu, G.X. Cai, C.H. Zhou, Eur. J. Med. Chem. 64 (2013) 329–344.
[21] C.Q. Sheng, W.N. Zhang, Curr. Med. Chem. 18 (2011) 733–766.
[22] Y. Wang, C.H. Zhou, Sci. Sin. Chim. 41 (2011) 1429–1456 (in Chinese).
[23] S.F. Cui, Y. Ren, S.L. Zhang, X.M. Peng, G.L.V. Damu, R.X. Geng, C.H. Zhou, Bioorg. Med. Chem. Lett. 23 (2013) 3267–3272.
[24] Y. Wang, G.L.V. Damu, J.S. Lv, R.X. Geng, D.C. Yang, C.H. Zhou, Bioorg. Med. Chem. Lett. 22 (2012) 5363–5366.
[25] Y.Y. Zhang, J.L. Mi, C.H. Zhou, X.D. Zhou, Eur. J. Med. Chem. 46 (2011) 4391–4402.
[26] Y.Y. Zhang, C.H. Zhou, Bioorg. Med. Chem. Lett. 21 (2011) 4349–4352.
[27] B. Fang, C.H. Zhou, X.C. Rao, Eur. J. Med. Chem. 45 (2010) 4388–4398.
[28] S.L. Zhang, G.L.V. Damu, L. Zhang, R.X. Geng, C.H. Zhou, Eur. J. Med. Chem. 55 (2012) 164–175.
[29] Q.P. Wang, J.Q. Zhang, G.L.V. Damu, K. Wan, H.Z. Zhang, C.H. Zhou, Sci. China. Chem. 55 (2012) 2134–2153.
[30] X.L. Wang, K. Wan, C.H. Zhou, Eur. J. Med. Chem. 45 (2010) 4631–4639.
[31] Y. Shi, C.H. Zhou, Bioorg. Med. Chem. Lett. 21 (2011) 956–960.
[32] F.F. Zhang, L.L. Gan, C.H. Zhou, Bioorg. Med. Chem. Lett. 20 (2010) 1881–1884.
[33] K. Wan, C.H. Zhou, Bull. Korean Chem. Soc. 31 (2010) 2003–2010.
[34] Y.J. Hu, Y. Liu, X.H. Xiao, Biomacromolecules 10 (2009) 517–521.
[35] J.J. Wei, L. Jin, K. Wan, C.H. Zhou, Bull. Korean Chem. Soc. 32 (2011) 229–238.
[36] L.L. Gan, B. Fang, C.H. Zhou, Bull. Korean Chem. Soc. 31 (2010) 3684–3692.
[37] S.L. Zhang, J.J. Chang, G.L.V. Damu, R.X. Geng, C.H. Zhou, Med. Chem. Commun. 4 (2013) 839–846.
[38] G.W. Zhang, P. Fu, L. Wang, M.M. Hu, J. Agric. Food Chem. 59 (2011) 8944–8952.
[39] X.L. Li, Y.J. Hu, Biomacromolecules 13 (2012) 873–880.
[40] National Committee for Clinical Laboratory Standards Approved standard Document, M27–A2, Reference Method for Broth Dilution Antifungal Susceptibility Testing of Yeasts, National Committee for Clinical Laboratory Standards, Wayne, PA, 2002.
[41] V.D. Suryawanshi, P.V. Anbhule, A.H. Gore, S.R. Patil, G.B. Kolekar, Ind. Eng. Chem. Res. 51 (2012) 95–102.
[42] J.R. Lakowicz, Principles of Fluorescence Spectroscopy, third ed., Springer, New York, 2006, pp. 11–12.
[43] S.S. Lehrer, Biochemistry 10 (1971) 3254–3263.
[44] G. Scatchard, Ann. N.Y. Acad. Sci. 51 (1949) 660–672.
[45] U.S. Mote, S.R. Patil, S.H. Bhosale, S.H. Han, G.B. Kolekar, Photochem. Photobiol. B. 103 (2011) 16–21.
[46] D.P. Ross, S. Subramanian, Biochemistry 20 (1981) 3096–3102.
[47] S.L. Zhang, J.J. Chang, G.L.V. Damu, B. Fang, X.D. Zhou, R.X. Geng, C.H. Zhou, Bioorg. Med. Chem. Lett. 23 (2013) 1008–1012.